Cloud droplet collision efficiency in electric fields

By HUBERT R. PLUMLEE[1] and RICHARD G. SEMONIN,[2] *Charged Particle Research Laboratory, Illinois State Water Survey and University of Illinois, Urbana, Illinois*

(Manuscript received, November 11, 1964)

ABSTRACT

A mathematical model describing the effects of forces acting on two spherical droplets immersed in a viscous medium is described. The model includes the interaction of the droplets with an externally applied electric field. The collision efficiencies between pairs of droplets ranging in size from 5 to 70 microns in radius are given as results of computations of the grazing trajectories of the smaller droplets relative to the larger drops in electric fields up to 10,000 volts per centimeter.

The collision efficiency for a given pair of droplets increases as the applied electric field increases. For example the collision efficiency of a 30 micron drop in relation to a 5 micron droplet increases 34.5 times when the horizontal field is changed from 0 to 3 600 volts per centimeter. Results of calculations are given to show how collision efficiencies vary as the orientation of the electric field is varied in relation to the axis of droplet motion. The results show that the maximum and minimum collision efficiencies occur with field orientations of 90 and 42 degrees respectively.

Introduction

The study of the all-water process of precipitation initiation has led to the concepts of collision, coalescence, and collection efficiencies between droplets of varying size. The collision efficiency is defined as the ratio of the cross-sectional area through which a droplet must pass for a collision to occur with a second droplet to the collision cross-section of the droplet pair. The coalescence efficiency is the fraction of colliding droplets which merge to form a larger drop. The collection efficiency is the product of the collision and coalescence efficiencies.

By the very definition of the coalescence efficiency, it can never exceed but may acquire any value less than or equal to unity. On the other hand, the collision efficiency, theoretically, is unbounded.

The collision efficiency of a pair of droplets is determined by the trajectories of the droplets while they are subjected to gravitational, aerodynamical, and electrical forces. To make the problem tractable for computing collision efficiencies in the presence of electric fields, the coordinate system for the calculation is fixed to the larger droplet (hereafter called the drop). Also it is assumed that the presence of the smaller droplet (hereafter called the droplet) does not disturb the fluid flow around the drop, since the drop-droplet interacting forces are not included. The trajectory of the droplet is determined by integrating the equation of motion

$$m_s \frac{d\mathbf{V}_s}{dt} = \mathbf{F}_a + \mathbf{F}_e + \mathbf{F}_g, \tag{1}$$

where m_s is the mass of the droplet, $\mathbf{V}_s$ is its velocity, $\mathbf{F}_a$ is the aerodynamical force, $\mathbf{F}_e$ is the electrical force, and $\mathbf{F}_g$ is the gravitational force. Theoretical methods are presented whereby each of the forces are determined and the collision efficiencies are obtained as a function of applied electric field.

Definition of collision efficiency

The collision efficiency is a measure of a cross-sectional area such that if the center of a droplet of radius a_s passes through this area the two droplets will collide. The diameter of the cross-sectional area is ascertained by computing

[1] Based upon a portion of a dissertation submitted in partial fulfillment for the degree of Doctor of Philosophy at the University of Illinois.

[2] Co-director, Charged Particle Research Laboratory.

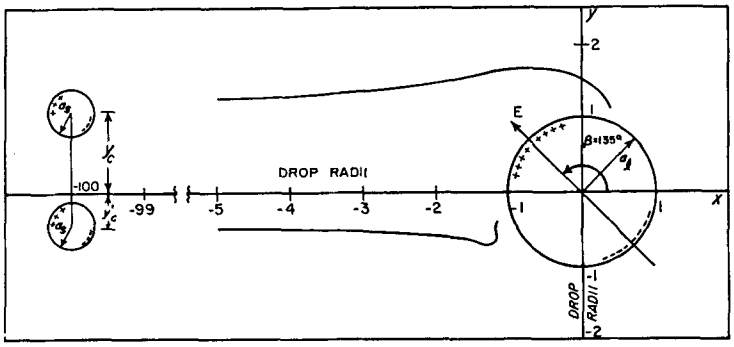

FIG. 1. The grazing trajectories in the half-planes ($y > 0$ and $y < 0$) for a 30 micron drop and a 5 micron droplet in an electric field oriented at $\beta = 135°$.

a pair of droplet trajectories which graze the collector drop on opposite sides of the axis of fall. The area through which droplets must pass to collide with a drop of radius a_l is given by

$$\frac{\pi}{4}(y_c - y_c')^2,$$

where y_c is the initial horizontal separation of droplet centers for the grazing trajectory in the upper half-plane of Fig. 1 and y_c' is the initial horizontal separation of droplet centers for the grazing trajectories in the lower half-plane. The definition of the collision efficiency, E_c, adopted in this work is the cross-sectional area, determined above, normalized by the collision cross-section of the droplet pair, $\pi(a_l + a_s)^2$. By this definition the collision efficiency is given by

$$E_c = \frac{\pi(y_c - y_c')^2}{4\pi(a_l + a_s)^2}. \qquad (2)$$

This definition takes into account non-symmetrical conditions which may occur when electrical forces act on the droplets. In addition, a collision efficiency of unity has a true physical meaning in the above definition. A drop of radius a_l will collide with all droplets of radius a_s when their centers lie within the drop-droplet pair collision cross-section.

Aerodynamics

The aerodynamical force, $\mathbf{F}_a$, in equation (1) is the drag force on a moving sphere in a viscous medium,

$$\mathbf{F}_a = -6\pi\mu a_s(\mathbf{V}_s - \mathbf{U})\, D_s, \qquad (3)$$

where μ is the viscosity of air, a_s is the radius of the droplet, $\mathbf{V}_s$ is the droplet velocity at a point in the fluid with velocity $\mathbf{U}$, and D_s is a coefficient to adjust the force for non-Stokesian droplets. The droplet is assumed to be of sufficiently small dimensions so that its effect on the fluid is negligible. The coordinate system is fixed to the drop so that the motions of the droplet and fluid are determined relative to the drop. Fig. 2 illustrates the coordinate system and the components of the forces and velocities shown are directed in the positive direction.

The vector stream velocity $\mathbf{U}$ in equation (3) may be written in component form as

$$\mathbf{U} = U_x\hat{x} + U_y\hat{y}, \qquad (4)$$

where $\hat{x}$ and $\hat{y}$ are unit vectors. The flow is assumed to be symmetrical about the x-axis.

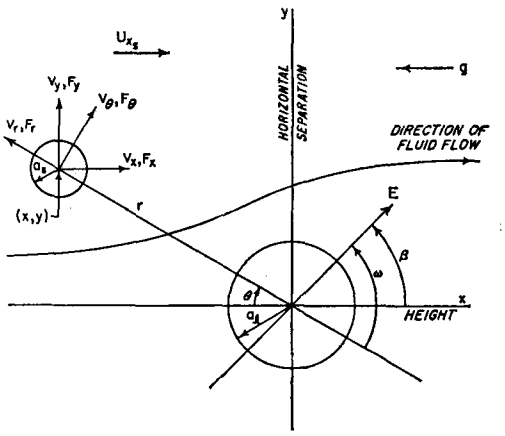

FIG. 2. Motion of a droplet in an electric field, E, relative to a fixed drop.

The r- and θ- components are obtained from the following relationships

$$\left.\begin{aligned} U_x &= -U_r \cos\theta + U_\theta \sin\theta, \\ U_y &= U_r \sin\theta + U_\theta \cos\theta, \end{aligned}\right\} \tag{5}$$

where θ is measured positively in a clockwise direction from the negative x-axis. The angular and radial components of the velocity in terms of a stream function ψ are

$$\left.\begin{aligned} U_r &= -\frac{1}{r^2 \sin\theta}\frac{\partial\psi}{\partial\theta}, \\ U_\theta &= \frac{1}{r\sin\theta}\frac{\partial\psi}{\partial r}. \end{aligned}\right\} \tag{6}$$

The stream function derived by PROUDMAN and PEARSON (1957) as a compromise between the OSEEN (1910) solution which satisfies the farfield boundary conditions and the STOKES (1851) solution which satisfies the no-slip condition at the surface of the sphere is used in this work. The stream function in terms of the Reynolds number, R_e, of the drop is given as

$$\begin{aligned} \psi = \frac{U_\infty}{4}\left(\frac{r}{a_l} - 1\right)^2 (1-\cos^2\theta) \\ \cdot\left[\left(1+\frac{3R_e}{16}\right)\left(2+\frac{a_l}{r}\right) - \frac{3R_e}{16}\right. \\ \left.\cdot\left(2+\frac{a_l}{r}+\frac{a_l^2}{r^2}\right)\cos\theta\right], \end{aligned} \tag{7}$$

where r is the radius vector to the point (r, θ) in the fluid, and U_∞ is the undisturbed fluid flow. The Reynolds number is defined as $2\varrho_a U_\infty a_l/\mu$ where ϱ_a is the density of air at 20°C and standard pressure, and the other symbols are as defined previously. When the partial derivatives of this expression are substituted in equation (6), the velocity components are found to be

$$\left.\begin{aligned} U_r = \frac{U_\infty}{4}\left(1-\frac{a_l}{r}\right)^2\left[(1-3\cos^2\theta)\right. \\ \cdot\left(2+\frac{a_l}{r}+\frac{a_l^2}{r^2}\right)\frac{3R_e}{16} + 2\cos\theta \\ \left.\cdot\left(1+\frac{3R_e}{16}\right)\left(2+\frac{a_l}{r}\right)\right], \end{aligned}\right\} \tag{8}$$

$$\left.\begin{aligned} U_\theta = \frac{U_\infty}{4}\sin\theta\left(1-\frac{a_l}{r}\right)\left[\left(1+\frac{3R_e}{16}\right)\right. \\ \cdot\left(4+\frac{a_l}{r}+\frac{a_l^2}{r^2}\right) - \frac{3R_e}{16} \\ \left.\cdot\left(4+\frac{a_l}{r}-\frac{2a_l^3}{r^3}\right)\cos\theta\right]. \end{aligned}\right\} \tag{8}$$

The aerodynamical force necessary to obtain the trajectories from equation (1) is obtained by substituting equation (8) into the angular and radial component form of equation (3). The x- and y- components are given as

$$\left.\begin{aligned} F_{xa} &= -F_{ra}\cos\theta + F_{\theta a}\sin\theta, \\ F_{ya} &= F_{ra}\sin\theta + F_{\theta a}\cos\theta, \end{aligned}\right\} \tag{9}$$

which is the form most convenient for computer use.

As discussed in the foregoing, the problem of two moving spheres was simplified by assuming that the fluid containing the droplet was flowing around a stationary drop. To solve the two-body problem, it was necessary to determine the flow of the fluid around the droplet. HOCKING (1959) estimated that the ratio of droplet radius to drop radius should be approximately one-tenth or less so that the mutual interaction of the flow patterns could be neglected. A comparison of the collision efficiencies of the present work with Hocking's and with SHAFRIR and NEIBURGER's (1963) is presented in Fig. 3 and shows that the ratio of one-tenth is more conservative than necessary for most cloud physics considerations.

Electrostatics

If water droplets are considered to be conducting spheres, the derivation of the electrostatic forces acting on them is simplified. Since the droplets to be considered are small and travel at moderate velocities, the assumption of the droplets being spheres will introduce only a small error in the results. From the equation of continuity of charge, $\nabla\cdot\mathbf{J} + \partial\varrho_\omega/\partial t = 0$, where $\mathbf{J}$ is the current density and ϱ_w is the charge density in the water, the relaxation time of the charge distribution in water can be derived in the following manner. Since $\mathbf{J} = \sigma\mathbf{E}$ where σ is the conductivity of water, then the continuity equation reduces to $\sigma\nabla\cdot\mathbf{E} + \partial\varrho_\omega/\partial t = 0$. But

$\nabla \cdot \mathbf{E} = \varrho_w/\varepsilon$ where ε is the permittivity of water; therefore, $\sigma\varrho_w/\varepsilon + \partial\varrho_w/\partial t = 0$. The charge density is proportional to $\exp(-\sigma t/\varepsilon)$ where the time constant, ε/σ, is the relaxation time for charge transfer in the material. For distilled water, the relaxation time is of the order of 100 microseconds. The charge density, thus the electric field intensity within the drop, decreases rapidly to zero with increasing time. This expresses the well-known fact that the field within a conductor is zero and justifies the assumption that water can be considered to be a conducting material.

DAVIS (1964) solved for the forces acting on two conducting rigid spheres when a uniform electric field, E, is present. He used a bispherical coordinate system as described by MORSE and FESHBACH (1953) and determined the surface charge densities, σ_s and σ_l, on the conducting spheres. The force acting on the droplet in the MKS system of units was computed by integrating the surface stress $\sigma_s^2/2\varepsilon_0$ over the surface of the droplet where ε_0 is the permittivity of free space.

The force on the droplet written in a convenient form for programming on a digital computer is given by

$$\mathbf{F}_e = F_{xe}\hat{x} + F_{ye}\hat{y}, \tag{10}$$

where
$$\left.\begin{aligned} F_{xe} &= -F_{re}\cos\theta + F_{\theta e}\sin\theta, \\ F_{ye} &= F_{re}\sin\theta + F_{\theta e}\cos\theta. \end{aligned}\right\} \tag{11}$$

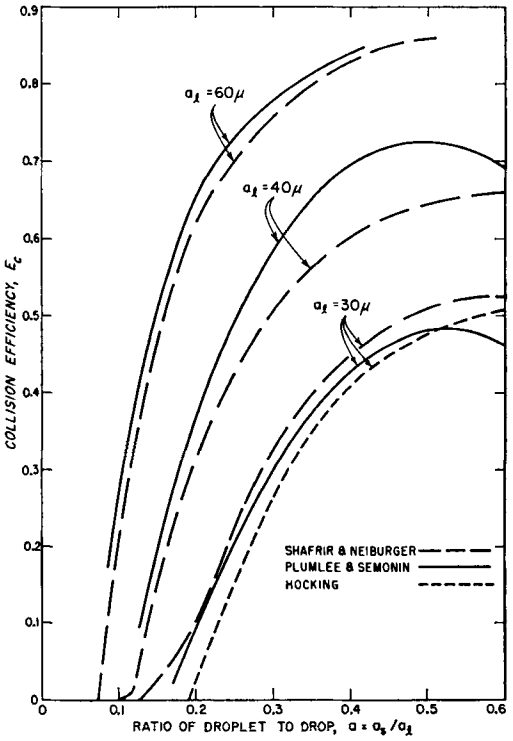

FIG. 3. Comparison of collision efficiencies as calculated by various authors.

From the rearranging of Davis' solutions of the smaller sphere, the components of the force acting in the r- and θ- directions are given by

$$\left.\begin{aligned} F_{re} &= 4\pi\varepsilon_0 A^2 \sum_{n=0}^{\infty} S_n\{(2n+1)S_n - (n+1)[\exp(2\mu_s)+1]S_{n+1}\}\exp[(2n+1)\mu_s] \\ &+ 8\pi\varepsilon_0 A^2 E^2 \sin^2\omega \sum_{n=0}^{\infty} n(n+1)T_n\{(2n+1)T_n - (n+2)[\exp(2\mu_s)+1]T_{n+1}\}\exp[(2n+1)\mu_s], \\ F_{\theta e} &= 4\pi\varepsilon_0 A^2 E \sin\omega[\exp(2\mu_s)-1]\sum_{n=0}^{\infty}(n+1)\{nS_{n+1}T_n - (n+2)S_nT_{n+1}\}\exp[(2n+1)\mu_s]. \end{aligned}\right\} \tag{12}$$

The coefficients are given as

$$\left.\begin{aligned} S_n &= \frac{E(2n+1)\cos\omega\left\{\exp[(2n+1)\mu_l+1] - \left(\frac{\phi_s}{A}\right)\right\}\exp[(2n+1)\mu_l] + \left(\frac{\phi_l}{A}\right)}{\exp[(2n+1)\mu_0]-1}, \\ T_n &= \frac{1-\exp[(2n+1)\mu_l]}{1-\exp[(2n+1)\mu_0]}. \end{aligned}\right\} \tag{13}$$

The potentials of each sphere due to both the induced charges, Q_l and Q_s, and the net charges, q_l and q_s, are

$$\left.\begin{aligned}\phi_l &= P_{ll}(q_l - 8\pi\varepsilon_0 A^2 E Q_l \cos\omega) + P_{ls} \\ &\quad \cdot (q_s - 8\pi\varepsilon_0 A^2 E Q_s \cos\omega), \\ \phi_s &= P_{sl}(q_l - 8\pi\varepsilon_0 A^2 E Q_l \cos\omega) + P_{ss} \\ &\quad \cdot (q_s - 8\pi\varepsilon_0 A^2 E Q_s \cos\omega).\end{aligned}\right\} \quad (14)$$

The coefficients of induction are

$$\left.\begin{aligned}P_{ll} &= \frac{C_{ss}}{C_{ll}C_{ss} - C_{ls}^2}, \\ P_{ls} = P_{sl} &= \frac{C_{ls}}{C_{ll}C_{ss} - C_{ls}^2}, \\ P_{ss} &= \frac{C_{ll}}{C_{ll}C_{ss} - C_{ls}^2},\end{aligned}\right\} \quad (15)$$

where the coefficients of capacitance are

$$\left.\begin{aligned}C_{ll} &= 8\pi\varepsilon_0 A \sum_{n=0}^{\infty} \frac{\exp[(2n+1)\mu_s]}{\exp[(2n+1)\mu_0] - 1}, \\ C_{ls} = C_{sl} &= 8\pi\varepsilon_0 A \sum_{n=0}^{\infty} \frac{1}{\exp[(2n+1)\mu_0] - 1}, \\ C_{ss} &= 8\pi\varepsilon_0 A \sum_{n=0}^{\infty} \frac{\exp[(2n+1)\mu_l]}{\exp[(2n+1)\mu_0] - 1}.\end{aligned}\right\} \quad (16)$$

The induced charges are

$$\left.\begin{aligned}Q_l &= 8\pi\varepsilon_0 A^2 \sum_{n=0}^{\infty} (2n+1) \frac{\exp[(2n+1)\mu_s] + 1}{\exp[(2n+1)\mu_0] - 1}, \\ Q_s &= -8\pi\varepsilon_0 A^2 \sum_{n=0}^{\infty} (2n+1) \\ &\quad \cdot \frac{\exp[(2n+1)\mu_l] + 1}{\exp[(2n+1)\mu_0] - 1},\end{aligned}\right\} \quad (17)$$

where

$$\left.\begin{aligned}&\exp(\mu_l) = \frac{C_l + A}{a_l}; \quad \exp(\mu_s) = \frac{C_s + A}{a_s} \\ &\mu_0 = \mu_l + \mu_s \\ &A = (C_l^2 - a_l^2)^{\frac{1}{2}} \\ &C_l = (r^2 + a_l^2 - a_s^2)/2r \\ &C_s = (r^2 + a_s^2 - a_l^2)/2r\end{aligned}\right\} \quad (18)$$

In the above equations, E is the applied electric field, ω is the angle between the electric field and the line joining the centers as illustrated in Fig. 2, and q_l and q_s are the net charges on the drop and droplet respectively. For the work reported here, the droplets are uncharged and q_l and q_s are zero.

Equations of motion

The various forces acting on the droplet are determined from the foregoing analyses. Since the negative x-axis is selected as the direction of vertical fall, the gravitational force, $m_s g$, acts on the droplet in the negative x-direction as shown in Fig. 2.

The equations of motion including the various forces are written in component form as

$$\left.\begin{aligned}m_s \frac{dV_{xs}}{dt} &= -6\pi\mu a_s (V_{xs} - U_x) D_s - m_s g + F_{xe}, \\ m_s \frac{dV_{ys}}{dt} &= -6\pi\mu a_s (V_{ys} - U_y) D_s + F_{ye}, \\ \frac{dx_s}{dt} &= V_{xs}, \\ \frac{dy_s}{dt} &= V_{ys}.\end{aligned}\right\} \quad (19)$$

These equations of motion were solved by the use of a digital computer and a numerical integrating routine first described by NORDSIECK (1962). The routine incorporated automatic starting and automatic selection and revision of the integration step. To start the integration, only the initial conditions, a specified accuracy of integration, and a logical elementary integration step are necessary. At small distances from the drop where changes in the motion of the droplet are greatest, the integration step is automatically shortened to obtain a solution of the given accuracy.

The initial velocities of the drop and droplet are determined by computing the terminal velocity of each when gravity acts on the masses. Since the center of the drop is assumed as the origin of a fixed coordinate system, the initial velocity of the droplet is the difference between the terminal velocities of the two droplets. The initial vertical separation for each trajectory is taken as 100 drop radii. At this separation, there is very little interaction between the disturbed fluid around the drop and the droplet. The initial horizontal separation of the first trajectory is taken as one drop radius.

Discussion of results

The collision efficiencies for pairs of droplets when either a horizontal or a vertical electric field is present are shown in Figs. 4, 5, and 6. The increase in the collision efficiency due to an applied electric field is a result of an induced nonuniform charge distribution on the surfaces of the two droplets. The interaction of the two charge distributions can either be attractive or repulsive depending on the orientation of the applied field and the relative position of the droplets. If only the dipole interaction is considered, the regions of attraction and repulsion can be determined as illustrated by LINDBLAD and SEMONIN (1963).

The results given in Figs. 4, 5, and 6 show that the influence of the fair weather atmospheric electric field cannot contribute to the collision efficiency of the drop-droplet pairs considered in this study. The normal fair weather electric field is of the order of one volt per centimeter whereas the major changes in the efficiency of collision occur at electric field intensities which are orders of magnitude greater.

The trajectories for the 30 and 5 micron droplet pair are shown in Fig. 7. The effect of

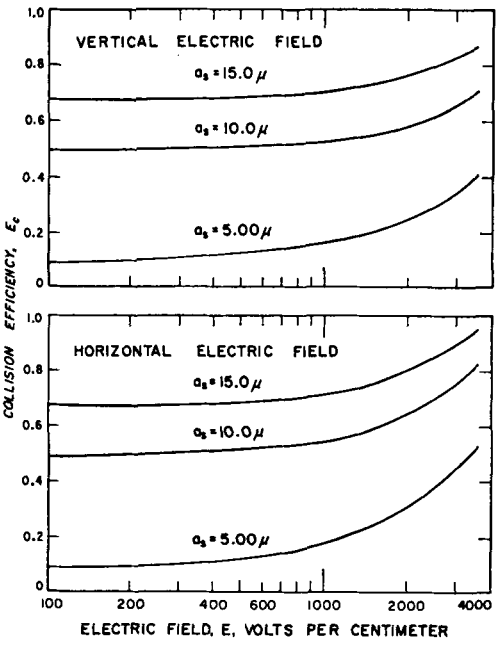

FIG. 5. Collision efficiency curves for a 40 micron drop with 5, 10, and 15 micron droplets.

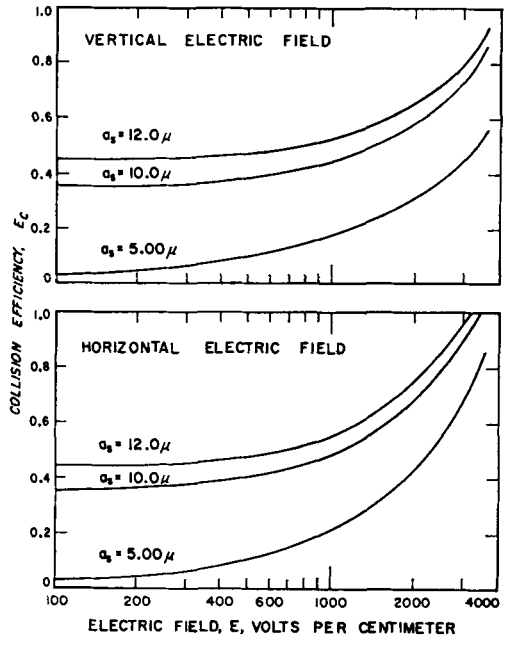

FIG. 4. Collision efficiency curves for a 30 micron drop with 5, 10, and 12 micron droplets.

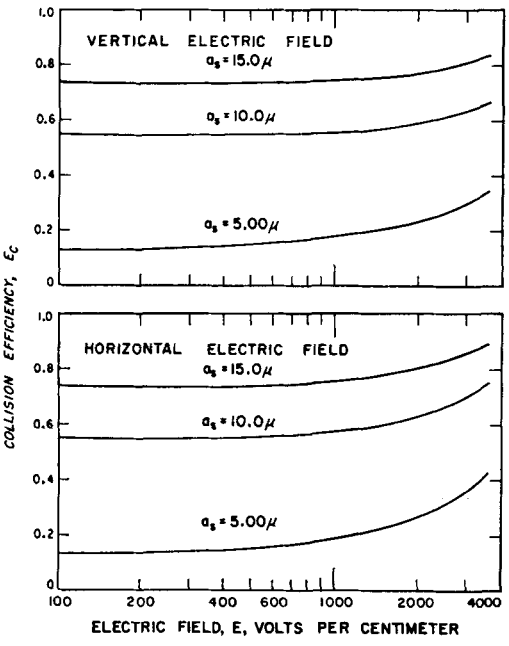

FIG. 6. Collision efficiency curves for a 50 micron drop with 5, 10, and 15 micron droplets.

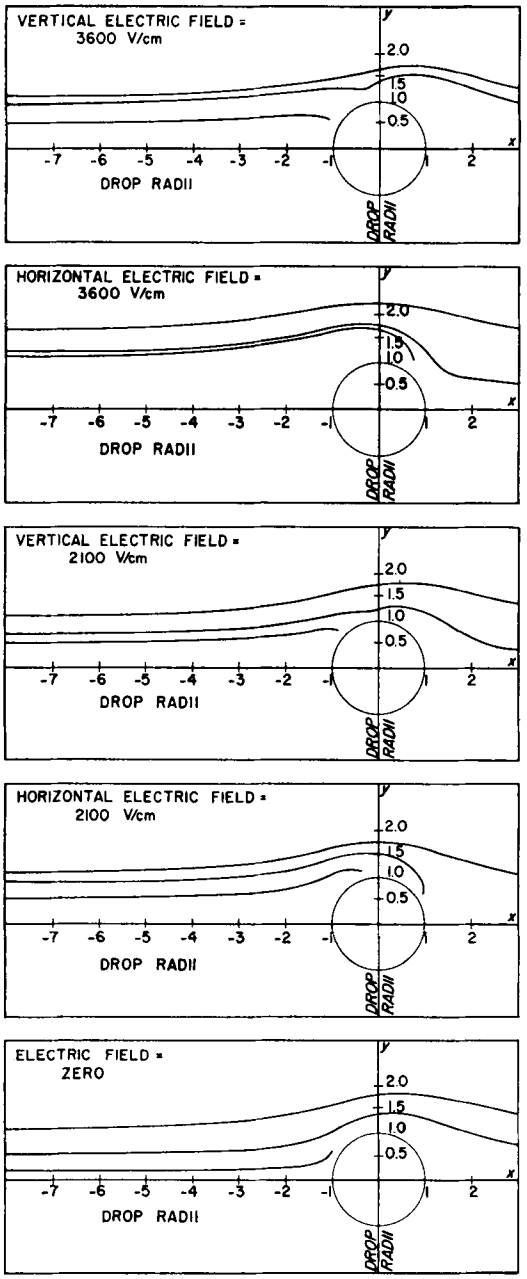

FIG. 7. Trajectories for a 5 micron droplet moving toward a 30 micron drop.

a region of repulsion about the y-axis on the trajectories is illustrated for the case of vertically applied electric fields. The initial trajectory of the droplet is toward the drop but it changes its direction of travel after entering this region of repulsion. The horizontally applied electric fields have a region of attraction about the y-axis and result in pulling the droplet into the back side of the drop for certain initial conditions of the droplet.

It is observed from Figs. 4, 5, and 6 that the horizontally applied electric fields produce the largest increase in collision efficiencies and the efficiencies are greatest for the 30 and 5 micron droplet pair. A horizontal electric field of 3 600 volts per centimeter increases the collision efficiency of a 30 and 5 micron pair by a factor of 34.5 compared to 5.6 for the 40 and 5 micron pair and 5.0 for the 50 and 5 micron pair. Thus, the collision efficiency curves flatten as the collector drop increases in size. This is due to the large difference between the relative velocities of the drop and droplet which does not allow a sufficient time for the electrical force to bring the pair together.

The effect of the orientation of the applied electric field is seen in Figs. 8 and 9 which show the change in the collision efficiency for various droplet pairs as a function of the angle β between the electric field, **E**, and the x-axis. The angle β, in Fig. 2, is measured positively in the counterclockwise direction and the effects are symmetric for an orientation about the y-axis where β is equal to either 90° or 270°. The largest collision efficiencies occur approximately in the range $50° < \beta \leq 90°$ and the lowest collision efficiency occurs for β approximately equal to 42°. The maximum collision efficiency occurs

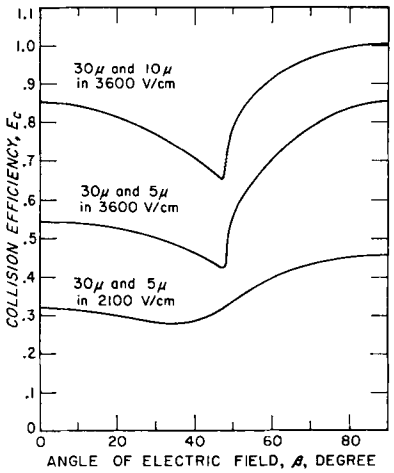

FIG. 8. Change in collision efficiency of droplet pairs for various orientations of electric fields.

TABLE 1. *Collision efficiencies for droplets for strong electric fields.*

Droplet Pair	Vertical Field			Horizontal Field		
	3 600V/cm	6 000V/cm	10,000V/cm	3 600V/cm	6 000V/cm	10,000V/cm
30μ and 5μ	0.5475	0.9624	1.7315	0.8540	1.4935	2.747
40μ and 5μ	0.4038	0.6433	1.0923	0.5368	0.8854	1.5190
50μ and 5μ	0.3433	0.5095	0.8200	0.4316	0.6729	1.0974

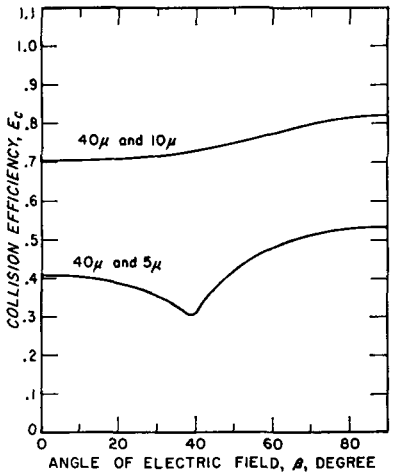

FIG. 9. Change in collision efficiency of droplet pairs for various orientations of electric fields at 3 600 volts per centimeter.

for β equal to 90°, i. e., a horizontally applied electric field.

Collision efficiencies for electric fields of 6 000 and 10,000 volts per centimeter are given in Table 1. For these very large electric fields, collision efficiencies greater than unity are calculated. Although such large fields are not commonly measured in clouds, it does seem reasonable that they may exist in very active clouds where lightning is present.

Conclusions

The collision efficiencies for uncharged cloud droplets of the sizes considered increase with an applied electric field. The maximum increase results for β equal to 90°, i. e., a horizontally applied electric field and the minimum increase results for β equal to 42°. For a given droplet size with or without electric fields present, the collision efficiency decreases as the drop size increases. However, for a given drop size the collision efficiency increases as the droplet size increases. If the strength of the applied electric field becomes high enough, the collision of cloud droplets can exceed unity.

Acknowledgements

We would like to acknowledge the assistance of Mr. E. Hassler, and Mr. N. Lindblad for discussions during the initial formulation of the problem. Special thanks are due Professor C. D. Hendricks, Co-Director CPRL who acted as thesis advisor for one of us.

This work was supported by U. S. Army Electronic Research and Development Laboratory grant AMC-63-G2 and National Science Foundation Grant NSF-GP2528. The use of the University of Illinois 7094-1401 computing system was partially supported by National Science Foundation grant NSF-GP700.

REFERENCES

DAVIS, M. H., 1964, Two Charged Spherical Conductors in a Uniform Electric Field; Forces and Field Strength, *Quart. J. of Mech. and Appl. Math.*, Vol. 17, Pt. 4, p. 499.

HOCKING, L. M., 1959, Three-dimensional Viscous Flow Problems Solved by the Stokes and Oseen approximation, *Ph. D. Thesis*, 100 pp. *University of London.*

LINDBLAD, N. R., and SEMONIN,R. G., 1963, Collision Efficiency of Cloud Droplets in Electric Fields, *J. of Geophys. Research*, Vol. 68, No. 4, p. 1051.

MORSE, P. M., and FESHBACH, H., 1953, Methods of Theoretical Physics, *McGraw-Hill Book Company, Inc.*, New York, p. 665 and 1298.

NORDSIECK, A. T., 1962, On Numerical Integration of Ordinary Differential Equations, *Math. Computation*, Vol. 16, p. 22.

OSEEN, C. W., 1910, Über die Stokessche Formel und über eine verwandte Aufgabe in der Hydrodynamik, *Ark. Mat. Astr. Fys.*, Vol. **6**, No. 29, p. 175.

PROUDMAN, I., and PEARSON, J. R. A., 1957, Expansions at Small Reynolds Numbers for the Flow Past a Sphere and a Circular Cylinder, *Journ. of Fluid Mech.*, Vol. **2**, p. 237.

SHAFRIR, U., and NEIBURGER, M., 1963, Collision Efficiencies of Two Spheres Falling in a Viscous Medium, *J. of Geophys. Gesearch*, Vol. **68**, No. 13, p. 4141.

STOKES, G. G., 1851, On the Effect of the Internal Friction of Fluids on the Motion of Pendulums, *Transactions, Cambridge Phil. Soc.*, Vol. **IX**, Pt. II, p. 8.